Finite Element Analysis of Interlayer Welds Loaded in Tension

The tensile deformation behavior of interlayer welds between elastic and plastic base metals is determined

BY G. A. HENSHALL, R. S. ROSEN, M. E. KASSNER AND R. G. WHIRLEY

ABSTRACT. The NIKE2D finite-element code has been used to analyze the states of stress and strain in cylindrical interlayer butt joints loaded in tension. A wide range of interlayer thickness-to-diameter ratios, t/d, applied stresses and material responses have been studied. For the case in which the base metals deform only elastically, the results of these analyses show several important differences from previously reported approximate analytical solutions and an earlier FEM study, particularly for small t/d. These differences have been attributed, at least partially, to nonuniform plastic straining in the interlayer. For base metals that plastically deform, the plastic strain in the interlayer produced by a given applied stress is significantly larger than for a similar weld between elastic base metals. For strain-hardening interlayers, this causes pronounced differences in the interlayer stress state compared with the elastic base metal case. Creep of the base metal induces time-dependent plastic deformation in the interlayer, even if the interlayer material alone does not creep. In this case, the rate at which the interlayer deforms is controlled by the creep rate of the base metal. The NIKE2D results are consistent with important experimental findings.

Introduction

Joining of similar and dissimilar materials often involves the use of thin interlayers. These interlayers may be produced by brazing (Refs. 1, 2), diffusion welding of metal foils (Ref. 3), diffusion welding of interlayer coatings produced by electroplating (Refs. 4, 5), or physical vapor-deposition processes (Refs. 5–7). Generally, the weld involves the use of a soft interlayer material, such as silver (Refs. 1, 2, 4–10) or copper (Ref. 3), to weld stronger base materials, such as maraging steel (Refs. 1,2,9,10), WC-Co (Ref. 3), U (Refs. 7, 8), or stainless steel (Refs. 7–10). Despite the low strength of the interlayer material, it has long been known that the welds may have ultimate tensile strengths much larger than that of the bulk interlayer material (Ref. 11). For example, the ultimate tensile strength (UTS) of silver-interlayer welds between maraging steel base metals has been reported to be as much as 760 MPa (110 ksi), while the maximum, or steady state, stress of the interlayer material itself is only about 260 MPa (37.3 ksi) (Ref. 9). The high tensile strength of interlayer welds is due to the mechanical constraint provided by the stronger base materials, which restricts transverse contraction of the interlayer (Refs. 1, 2,11–15). The constraint causes triaxial tensile stresses to develop within the joint, thus decreasing the effective stress in the interlayer and inhibiting plastic flow. The degree of mechanical constraint in the weld is known to increase with decreasing thickness-to-diameter ratio, t/d, of the interlayer. Higher joint strength is associated with higher constraint. If the base metal deforms plastically (Refs. 2, 8–10), the mechanical constraint is partially relieved, and the strength of the joint is degraded. Recent studies (Ref. 8) have shown that interlayer welds also exhibit time-dependent, or delayed, failure under sustained tensile loads. In this case, it was believed that time-dependent creep deformation of the base metal relieves the mechanical constraint and accelerates failure of the weld.

While the tensile behavior of interlayer welds is reasonably well understood qualitatively, particularly for thick interlayers, better quantitative predictions of the stress and strain state are needed for a complete understanding of thin interlayer welds. Considering a solid cylindrical tensile specimen geometry with the butt joint at the midplane of the cylinder, Orowan, *et al.* (Ref.11), derived a simple expression for the radial stress[1] within the interlayer as a function of the yield strength of the bulk interlayer material and t/d:

$$\sigma_r = \frac{\sigma_Y}{t}\left(\frac{d}{2} - r\right) \qquad (1)$$

This equation was originally derived by assuming ideal plastic behavior (*i.e.*, no strain hardening) of the interlayer, uniform (as a function of r) plastic strain within the interlayer, and that the base metal does not deform plastically. Results of the present investigation and an earlier finite-element study (Ref. 3) reveal significant deviation from Equation 1.

To gain a better understanding of the mechanical behavior of interlayer welds, Almond, *et al.* (Ref. 3), performed a finite-element analysis of WC-Co base metals welded with a Cu interlayer. The geometry of these butt joints was the same as that studied by Orowan, *et al.*, in deriving Equation 1. Qualitatively, the shape of the radial stress distribution was found to be similar to that described in Equation 1. Quantitatively, however, it was found

KEY WORDS

Finite Element Analysis
Interlayer Welds
Tensile Deformation
Tension-Loaded Welds
Stress Analysis
Diffusion Welds
Triaxial Stress
Finite-Element Code
Computer Modeling
Butt Joints

G. A. HENSHALL, R. S. ROSEN and R. G. WHIRLEY are with Lawrence Livermore National Laboratory, Livermore, Calif. M. E. KASSNER is with the Dept. of Mechanical Engineering, Oregon State University, Corvallis, Ore.

(1) The radial stress is normally used to characterize the stress state in the interlayer (e.g. Refs. 1, 11). Plasticity in the interlayer is accompanied by transverse contraction, which is opposed by the base metals. This produces a radial (and nearly equal hoop, Ref. 3) stress. There is, of course, a close relationship between σ_r and the hydrostatic stress, σ_H. Qualitatively, any conclusions made regarding σ_r apply also to σ_H (and the hoop stress).

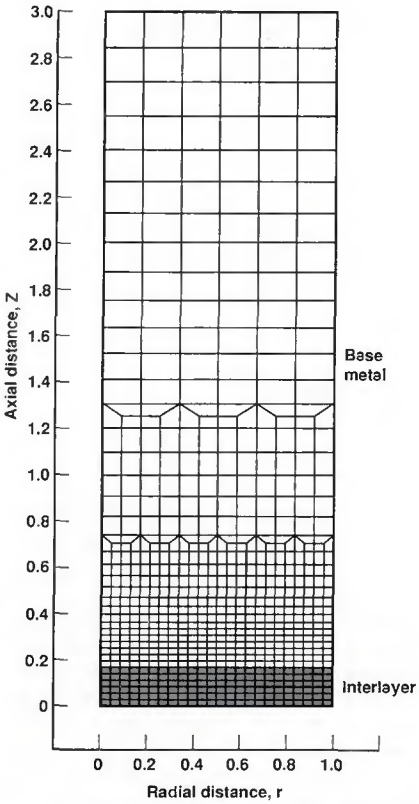

Fig. 1—The finite-element mesh used for NIKE2D simulations of an interlayer weld with a t/d ratio of 1/6.

that nonuniform plastic straining in the interlayer causes the σ_r distribution to deviate from the predicted linear behavior, producing σ_r values significantly larger than those predicted by Equation 1. The analysis of Almond, *et al.*, was limited, however, to large t/d ratios (1/3–1/6) and to elastically deforming base metals. Thus, smaller t/d ratios, such as those commonly employed in brazing and solid-state welding (Refs. 7–9,13), need to be examined.

To date, the quantitative effect of base-metal plasticity upon the mechanical behavior of the weld has not been determined, except in an approximate way (Ref. 2). Motivated by recent experiments concerning the fracture strength of interlayer welds between plastically deforming base metals (Refs. 8, 9), one of the goals of the present investigation was to evaluate the effects of base-metal plasticity on the stress and strain state in the interlayer. Of even greater concern was the time-dependent, or delayed, failure of interlayer welds reported earlier (Ref. 8). This subject has received far less attention than that of predicting the ultimate tensile strength of the welds. It has been shown (Refs. 8,10) that delayed failure can occur within several months at applied stresses as low as 17% of the UTS, demonstrating the importance of understanding the time-dependent behavior of the welds. The experimental results also show that creep of the base metal greatly accelerates the time-dependent failure of silver-interlayer diffusion welds. To understand delayed failure, it is necessary to have an accurate knowledge of the stress and strain state in the interlayer and an understanding of how creep of the base metal affects these quantities.

With this motivation, the goal of the present investigation was to use finite-element method (FEM) analyses to study the mechanical behavior of axially-loaded interlayer welds. First, for welds between elastically deforming base metals, the effect of t/d on the stress state within the interlayer was studied. It was found that, particularly for small t/d ratios, the stress state is significantly different from that predicted by Equation 1 and determined by Almond, *et al.* (Ref. 3). Next, the effect of time-independent plastic deformation in the base metal was examined to quantitatively compare the stress and strain within the interlayer with that for elastic base metal welds. Finally, time-dependent creep deformation of the base metal was simulated to demonstrate how creep of the base metal can control the behavior of the interlayer. This last analysis is particularly relevant to earlier work published by the authors (Ref. 8).

The Finite-Element Analysis

The FEM calculations were performed using the NIKE2D two-dimensional stress analysis code (Ref.16). NIKE2D is an implicit, finite-deformation, static/dynamic code that has been vectorized for maximum efficiency on vector-processor computers. Large problems can be solved in relatively short times, allowing much smaller t/d ratios to be studied than those reported by Almond, *et al.* (Ref. 3).

All the calculations were performed using quadrilateral four-node elements. The geometry modeled was that of a solid cylindrical rod with the interlayer weld placed in the center of the rod. Due to the axisymmetry of this geometry, a two-dimensional analysis of one-quarter of the rod was possible. With this geometry, the bottom of the mesh ($z = 0$) corresponds to the center plane of the interlayer, and the left edge of the mesh ($r = 0$) corresponds to the center axis of the cylindrical rod. The mesh used for a t/d ratio of 1/6 is shown in Fig. 1, and contains 672 elements and 728 nodes. The mesh used for the majority of the calculations was much finer because of the small t/d ratio of approximately 1/42. This geometry was chosen to correspond with the specimens used in previous experimental studies (Refs. 8–10), for which the diameter of the rod was 6.35 mm (0.25 in.) and the interlayer thickness was 0.152 mm (0.006 in.). Here, the model consisted of 2256 elements and 2355 nodes; calculations using an even finer mesh were performed to confirm spatial convergence.

Simulated loads were applied by prescribing a uniform tensile traction on the upper boundary of the mesh. Except for the creep simulations, the stress was increased continuously with time to its maximum value at the end of the simulation. For the case in which both the interlayer and the base metal were modeled as elastic-plastic materials, simulated loading to 689.5 MPa (100 ksi) using the 2256-element mesh took approximately 8 min of CPU time on a CRAY Y-MP computer. Use of various time-step sizes and convergence tolerances confirmed that proper numerical convergence had been achieved. Contour plots confirmed that the stress state was uniform and purely tensile at the top of the mesh for all applied stresses, demonstrating that end effects were not influencing behavior near the interlayer.

Three different material laws were used in the calculations. Elastic behavior was represented using linear isotropic elasticity theory. The elastic constants, E and ν, for the three different materials examined in this study, are given in Table 1. Time-independent plastic deformation was represented using isotropic von Mises plasticity theory. The experimentally determined effective stress vs. effective plastic strain curves for vacuum-annealed Type 304 stainless steel and the vapor-deposited interlayer silver are given in Fig. 2. The silver properties were determined by torsion tests of 150-μm-thick welds to avoid the mechanical constraint produced by tensile loading (Ref. 9). It is noteworthy that the yield strength and strain hardening rate of the interlayer silver are larger than for bulk-annealed polycrystalline silver, as discussed elsewhere (Ref. 9). The eight points shown on each curve were entered as material data for the NIKE2D code. Time-dependent creep deformation was represented using the primary creep law (Ref.17),

$$\bar{\varepsilon}_{cr} = A\bar{\sigma}^n \tau^m \qquad (2)$$

Table 1—Material Properties Used in the FEM Analyses

Material	E (MPa)	E (10^3ksi)	ν	A[a]	n	m
Maraging Steel	186	27.0	0.3	—	—	—
Annealed 304 Stainless Steel	193	28.0	0.29	8.71×10^{-14}	4.68	0.0647
Interlayer Silver	71	10.3	0.37	—	—	—

(a) For stress in MPa and time in seconds.

where $\bar{\varepsilon}_{cr}$ is the effective creep strain, $\bar{\sigma}$ is the effective stress and τ is time. The constants A, n and m for annealed 304 stainless steel deformed at ambient temperature are given in Table 1.

Numerical Results and Discussion

Elastic Base Metals

Figure 3 shows the effect of t/d on the radial stress distribution at the center plane of the interlayer ($z = 0$) for an applied stress of 345 MPa (50 ksi). The maraging steel properties were used in these calculations to model the base metal. Trends similar to those shown in Fig. 3 were observed for the axial, hoop and hydrostatic stresses. Figure 3A presents the results of calculations in which the interlayer was modeled as an ideal plastic[2] material, so that comparisons could be made with the predictions of Equation 1 for similar conditions. For t/d larger than about 1/15, Equation 1 predicts qualitatively correct behavior for the σ_r distribution in the interlayer; σ_r increases continuously as r decreases. In addition, the σ_r distribution is nearly linear for t/d = 1/10, and would probably be so for t/d = 1/6 if calculations could be performed for a truly ideal plastic interlayer (nonuniform strain hardening has occurred in the interlayer with $\bar{\sigma}$ ranging from 92.4 to about 98 MPa). For large t/d, the value of σ_r at the center axis ($r = 0$) increases as t/d decreases, as predicted by Equation 1. Quantitatively, however, for "thick" interlayers (t/d greater than about 1/15) the radial stresses computed by NIKE2D are significantly larger than those predicted by Equation 1. For example, the value of σ_r at $r = 0$ computed by Equation 1 is 462 MPa (σ_Y = 92.4 MPa) for t/d = 1/10. The value computed by NIKE2D is approximately 50% larger than this value. For strain-hardening thick interlayers, Almond, *et al.* (Ref.3), also found that Equation 1 underestimates the amount of constraint provided by the base metals.

For t/d ratios below about 1/15, the σ_r distribution predicted by NIKE2D does not even qualitatively resemble that given by Equation 1. The FEM results show that the stress distribution becomes much more uniform as t/d decreases. The radial stress near the center axis predicted by NIKE2D in this case is smaller than that predicted by Equation 1. In a much earlier study, Moffatt and Wulff (Ref.13) suggested that this would be the case for thin-interlayer welds. The NIKE2D results also show that a peak in the stress distribution develops at small t/d ratios, which becomes more localized near the OD as t/d decreases. This peak is associated with the nonuniform plastic deformation that occurs in the interlayer, which then leads to a local stress concentration. For example, for t/d = 1/6 and an applied stress of 345 MPa, the effective plastic strain is relatively uniform and so no peak is observed. For t/d = 1/42, however, the peak effective plastic strain near the OD is an order of magnitude larger than at the center axis, leading to the peak in the σ_r vs. r curve. It should be emphasized that, although the peak in the distribution at small t/d is perhaps the most striking feature of the stress distribution, the characteristic that is believed to be the most critical in controlling the behavior of the weld is that σ_r (as well as σ_H and $\bar{\sigma}$) is essentially uniform over most of the area of the interlayer. This conclusion stems from experimental results showing an essentially uniform distribution of microvoids on the fracture surface of failed thin interlayer welds (Refs. 10,13,18).

The deficiency of Equation 1 is also demonstrated by the fact that, for t/d less than about 1/10, the maximum radial stress decreases as t/d decreases (see Fig. 3A). Equation 1 predicts that σ_r always increases as t/d decreases. It is important to

(2) To avoid numerical difficulties, a small amount of strain hardening in the interlayer was simulated. For t/d ratios of 1/10 or less, the interlayer was assumed to yield (0.1% offset) at 92.4 MPa and to strain harden to 96 MPa at an effective plastic strain of 10%. For a t/d ratio of 1/6 it was necessary to allow the interlayer to harden to 100 MPa at a strain of 10% for the same yield stress.

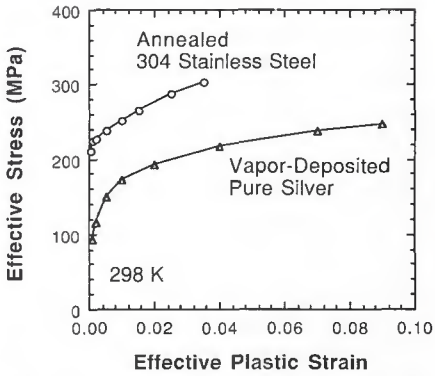

Fig. 2 — The (von Mises) effective stress vs. effective strain curves for annealed 304 stainless steel and vapor-deposited pure silver.

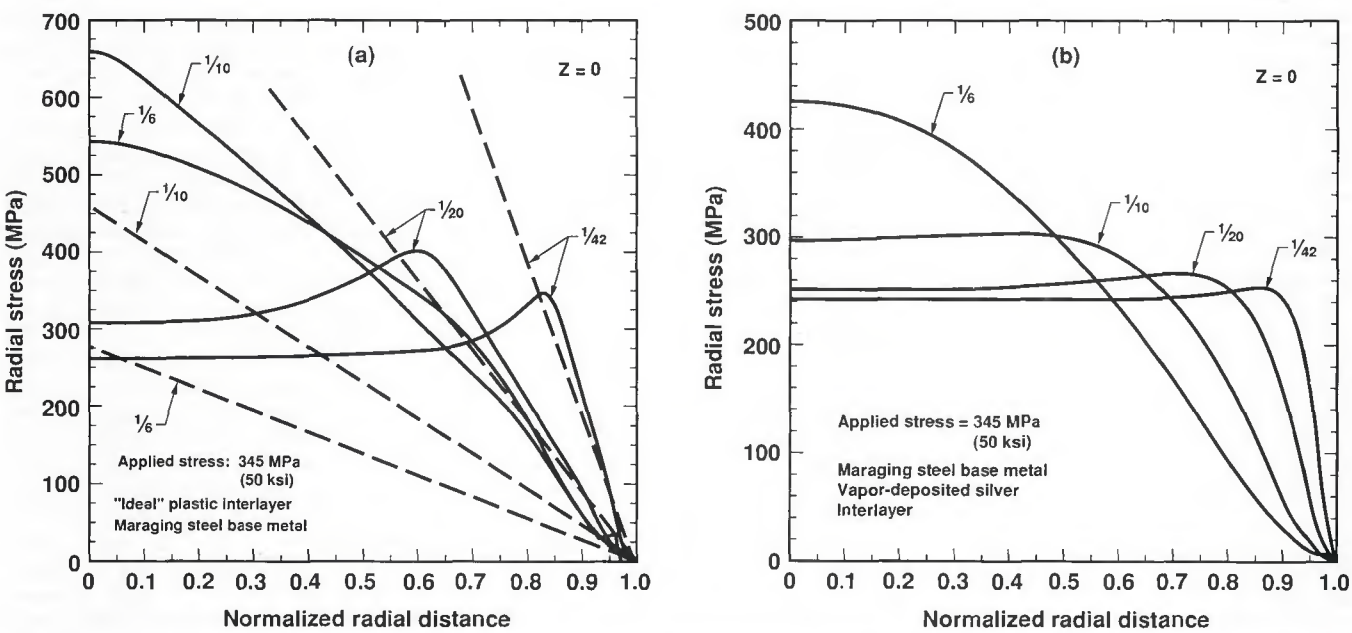

Fig. 3 — NIKE2D predictions (solid lines) of the effect of t/d on the radial stress distribution at the center plane of the interlayer (z = 0) for welds between maraging steel base metals subjected to an applied stress of 345 MPa (50 ksi). The predictions were made for: A — ideal plastic interlayers (the predictions of Equation 1 are given by the dashed lines); B — vapor-deposited pure-silver interlayers.

emphasize that the NIKE2D results do not imply that decreasing t/d decreases the constraint that the base metal produces within the interlayer. The analyses show that, as t/d decreases, a larger applied stress is needed to produce a given amount of plastic strain in the interlayer. This indicates that decreasing t/d increases the mechanical constraint in the interlayer, as expected from earlier investigations (Refs. 1–3).

The reason for the discrepancies between the analytical and NIKE2D results undoubtedly stems from the simplifying assumptions used to derive Equation 1. In particular, for a given value of z, a radially uniform strain state was assumed. The NIKE2D results indicate that this is not the case, with plastic deformation beginning near the OD and concentrating in this region as the applied stress increases[3]. This is not surprising since, physically, one would expect plastic flow to be more difficult in the center of the interlayer (r = 0) than near the OD because of the constraint from surrounding material. For an elastic base metal it is easy to understand how nonuniform plastic strain can lead to large stresses near the center axis for thick interlayers. Since the base metal deforms elastically, the deflections in the base metal are small. This implies that the interlayer/base-metal interface is essentially planar, even though the stresses may be concentrated in one region. (As shown in the next section, this is not the case for plastic base metals.) A planar interface means that the total (elastic plus plastic) strain across the thickness of the interlayer is essentially independent of r. Since the plastic strain in the interlayer is larger near the OD than near the center axis, the reverse must be true for the elastic strain. It is elastic strains that produce stress, therefore nonuniform plastic straining leads to a redistribution of stress such that the hydrostatic (or radial) stress is large near the center axis. For "thin" interlayer welds, the increase in plastic strain is localized very near the OD. Thus, the increased elastic strain and hydrostatic stress are localized to a region just inside that at which the plastic strain is concentrated, producing a peak in the stress distribution near the OD. Careful analysis of the NIKE2D results shows that the predicted hydrostatic stress peaks are indeed at radial positions just inside those for which the plastic strain is a maximum.

Figure 3B shows the effect of t/d on the σ_r distribution at the center plane (z = 0) of a strain-hardening interlayer for an applied stress of 345 MPa (50 ksi). In this case, the flow curve shown in Fig. 2 for the vapor-deposited silver was used to model the behavior of the interlayer. For the thick joint, t/d = 1/6, the results are qualitatively similar to those for the ideal plastic interlayer. However, σ_r is substantially smaller at $r = 0$ for the strain-hardening interlayer than for the ideal plastic one. For all t/d ratios the σ_r distribution is more uniform than for the ideal plastic interlayer. Strain hardening makes the plastic strain distribution more uniform (since a higher effective stress is needed to continue plastic flow as the plastic strain increases), which leads to a more uniform stress distribution. In addition, for a given applied stress, the larger effective stress produced by strain hardening directly results in a lower hydrostatic stress, and thus a lower radial stress. As in Fig. 3A, the general trend of increasing σ_r with decreasing radial distance is predicted for the thick joint. Deviation from the linear distribution predicted by Equation 1 is again observed, however. It is noteworthy that departures from a linear σ_r distribution were also observed experimentally in the compression of soft interlayer materials between rough cylindrical platens (Ref. 19). As discussed by Moffatt and Wulff (Ref.13), the compressive mode of deformation should produce stress distributions similar, except opposite in sign, to those studied in the present investigation. The NIKE2D results for t/d = 1/6 are also similar to those of Almond, *et al.* (Ref. 3), for the same weld geometry (but different material properties). Both FEM investigations indicate that, for thick interlayers, the σ_r (and σ_H) distribution is nonlinear and that σ_r at the center axis is substantially larger than that predicted by Equation 1.

In a manner similar to that shown in Fig. 3A, the σ_r distribution for the strain-hardening interlayers exhibits significant deviations from the behavior predicted by Equation 1 as t/d decreases. First, for the strain-hardening interlayer, σ_r near the center axis, or the "plateau" value, decreases as t/d decreases for all t/d ratios investigated. Thus, σ_r is much smaller than that which would be predicted based on thick joint results and the assumption that Equation 1 is at least qualitatively correct. Again, this does not imply that the constraint decreases with decreasing t/d. Rather, small t/d ratios result in small nonuniform plastic strains for a given applied stress. Second, small t/d ratios favor a more uniform stress distribution with a peak near the OD, which becomes more localized as t/d decreases. The change from "thick-joint" behavior (qualitatively similar to Equation 1) to that of "thin-joint" behavior (not qualitatively similar to Equation 1) occurs at larger t/d ratios for the strain-hardening interlayer than for the ideal plastic interlayer. The peak in the σ_r distribution is again associated with the localization of plastic strain near the OD as t/d decreases. Strain hardening in the interlayer makes these peaks smaller than for the ideal plastic material because of the more uniform strain distribution produced. Thus, the assumption made by Almond, *et al.* (Ref. 3), that the shape of the stress distribution is independent of t/d, which was based on calculations using only large t/d values, does not hold for t/d less than about 1/6. Again, however, the most important characteristic of the σ_r distribution for small t/d is that the stress is essentially uniform over most of the area of the interlayer.

Some experimental evidence exists to support the NIKE2D predictions of a relatively uniform stress distribution for thin joints. Moffatt and Wulff (Ref.13) observed that the fracture surfaces of thin interlayer welds exhibit voids of uniform size over most of the area, implying that the hydrostatic stress distribution is nearly uniform. Similar observations have been made recently in silver-interlayer diffusion welds with a t/d ratio of 1/42 by Rosen and Kassner (Ref. 9) for tensile fracture, and by Kassner, *et al.* (Ref.10), for creep rupture. NIKE2D calculations of a uniform σ_H distribution for t/d = 1/42, which is qualitatively the same as that of the σ_r distribution shown in Fig. 3B, are consistent with these experimental observations.

Figures 3A and B also show that the radial stress state becomes insensitive to changes in t/d for low t/d ratios. This fact could help explain why increases in the UTS of the weld with decreasing t/d tend to plateau as t/d becomes very small (Refs. 5,13,14, 20). Previous investigators believed that this phenomenon was due only to discontinuities (porosity, flatness, etc.) in very thin welds. While such problems certainly do occur and contribute to a plateau (or decrease) in the UTS, the present results indicate that a plateau in strength would occur even if a perfect weld could be made. This conclusion is supported by recent experiments by Rosen (Refs. 9,18). Silver-interlayer welds between maraging steel base metals were fabricated with t/d ratios of approximately 1/6, 1/42 and 1/125. The UTS of the weld with t/d = 1/6 was significantly less than that of the other welds, as expected. However, the UTS of welds with t/d = 1/125 was essentially the same as that for welds with t/d = 1/42, suggesting a similarity in the stress and strain states. Similarly, the creep-rupture times for silver-interlayer welds with t/d = 1/6 were considerably less than for welds with t/d = 1/42 or 1/125 (Ref. 18). The creep-rupture times for welds with t/d = 1/125 were essentially the same as for those with t/d = 1/42, again implying that the stress and strain states were nearly equivalent.

One obvious use of the FEM results would be to predict the UTS of the welds.

(3) In their FEM analysis, Almond, et al. (Ref.3), also reported that plastic straining began near the OD and spread toward the center axis in a strain-hardening interlayer for t/d ≥ 1/6. This fact was used to explain why the constraint computed by FEM is greater than that predicted by Equation 1.

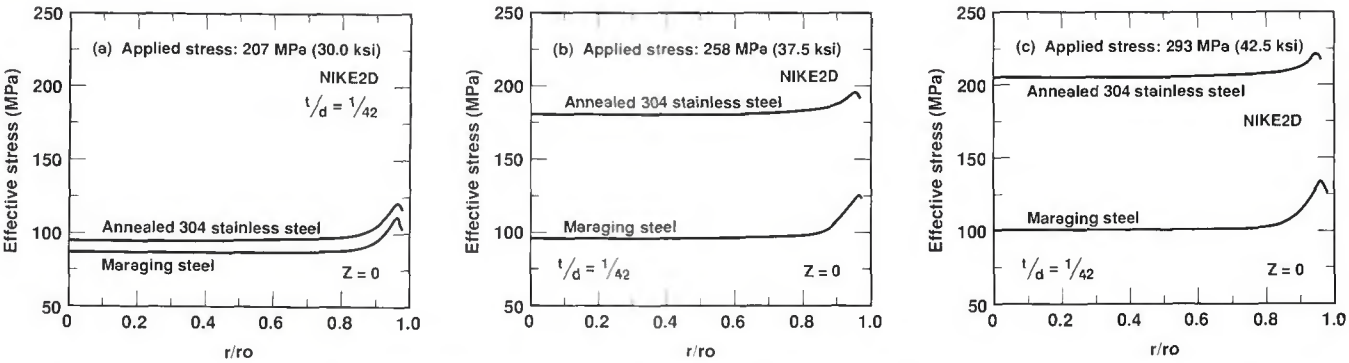

Fig. 4 — NIKE2D predictions of the (von Mises) effective stress at the center plane of the interlayer (z = 0) for silver-interlayer welds (t/d = 1/42) between maraging steel and annealed 304 stainless steel base metals at applied stresses of: 207 MPa (30.0 ksi), 258 MPa (37.5 ksi), and 293 MPa (42.5 ksi).

This is a difficult problem, however, because the correct failure criterion must be known. A full investigation of this subject is beyond the scope of this paper, but a preliminary study was performed for welds using the elastically deforming maraging steel base metal. In this case, failure is controlled only by the behavior of the interlayer (Refs. 2,10,18), so fracture would be expected to occur when the stress/strain state within the interlayer reaches some critical condition, regardless of the t/d ratio. These criteria would assume, of course, that failure is not controlled by delamination due to a degraded interface. Many ductile failure criteria have been reported in the literature. One relevant theory that includes the effect of a large hydrostatic tensile stress has been derived by Rice and Tracey (Ref. 21) and further developed by Hancock and MacKenzie (Ref. 22). Following Hancock and MacKenzie, the failure strain is related to the stress state through the parameter D, where D is defined:

$$D = 3\sigma_H/2\bar{\sigma} \qquad (3)$$

If D is the relevant parameter controlling ductile fracture of the welds, one would expect equivalent D values at the UTS, independent of t/d. Rosen and Kassner (Ref. 9) have found that for silver-interlayer welds between maraging steel base metals, the UTS is 448 MPa for t/d = 1/6.25, and 655 MPa for t/d = 1/42. NIKE2D simulations for these two types of welds loaded to their respective ultimate tensile stresses give the following results: at z = r = 0, D for the thick joint is 6.14, and for the thin joint D is 6.04. The similarity in these values is consistent with the expectation that the critical value of D should be independent of t/d. These results, however, may be fortuitous. For example, Rosen and Kassner (Ref. 9) reported that the fracture strain for silver-interlayer welds with t/d = 1/6.25 was much larger than for welds with t/d = 1/42, shedding some doubt on the significance of D. The discrepancy in fracture strains may be due, however, to differences in the strain needed to nucleate microvoids, which is not associated with D (Ref. 22). In any case, a more thorough investigation would be needed to make any firm conclusions regarding prediction of the UTS using FEM analysis.

Time-Independent Plasticity in the Base Metal

Although several experimental investigations have revealed the presence of plasticity in the base metal (Refs. 2, 8–10), a quantitative assessment of its effect on the stress state within the interlayer has not been performed. The finite-element method allows plasticity in the base metal, including concomitant work hardening of the base metal and the interlayer, to be directly included in the analysis. Therefore, NIKE2D simulations were performed for an interlayer weld (t/d = 1/42) in which both the interlayer and the base metal were modeled as von Mises elastic-plastic materials. The vapor-deposited silver properties were used for the interlayer and the annealed 304 stainless steel properties were used for the base metal (see Fig. 2 and Table 1) since experimental data were available for these welds. Figure 4 shows the effective stress at the center plane of the silver interlayer as a function of the normalized radial distance, r/r_o, at three different applied stresses for welds between elastic (maraging steel) and plastic (annealed 304 stainless steel) base metals. Figure 5 shows the corresponding effective plastic strains as a function of r/r_o at the center plane of the interlayer and in the stainless steel base metal just above the interface. The slight difference in E and ν for the two base metals cannot account for the large differences in behavior. For applied stresses below that at which the 304 stainless steel significantly deforms plastically, the stress states in the interlayer are essentially identical for the two types of base metal. Thus, the differences in behavior between the two welds at the applied stresses shown are caused by plastic deformation in the

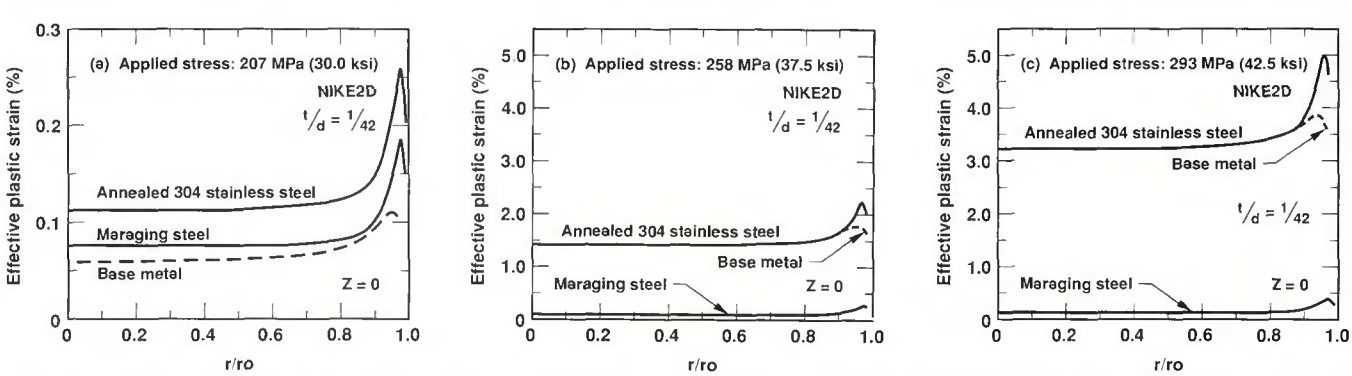

Fig. 5 — NIKE2D predictions of the effective plastic strain at the center plane of the interlayer (z = 0) for silver-interlayer welds (t/d = 1/42) between maraging steel and annealed 304 stainless steel base metals at applied stresses of: 207 MPa (30.0 ksi), 258 MPa (37.5 ksi), and 293 MPa (42.5 ksi). The effective plastic strain in the stainless steel base metal just above the interface is shown as a dashed line.

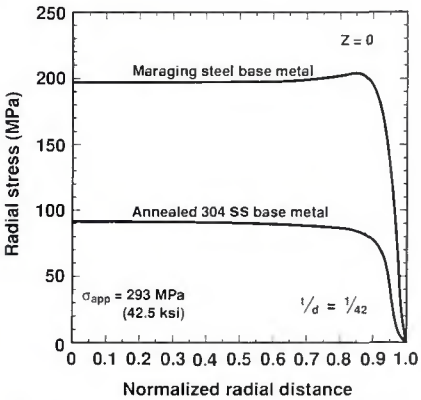

Fig. 6 — The radial stress distribution at the center plane of the interlayer predicted by NIKE2D for silver-interlayer welds (t/d = 1/42) between maraging steel and annealed 304 stainless steel base metals deformed at an applied stress of 293 MPa (42.5 ksi).

304 stainless steel base metal.

The major effect of plasticity in the base metal is to partially relieve the mechanical constraint, allowing the interlayer to plastically deform much more than if the base metal deforms only elastically, as shown in Fig. 5. For an ideal plastic interlayer, the increased plastic strain does not change the effective stress within the interlayer. In this case, the interlayer stress state for welds using plastically deforming base metals is the same as that for welds using elastically deforming base metals loaded to the same far-field stress. Strain hardening of the interlayer, however, directly results in an increase in $\bar{\sigma}$ with increasing effective plastic strain. Therefore, the stress distribution within the interlayer for a weld between plastically deforming base metals will differ from that for a weld between

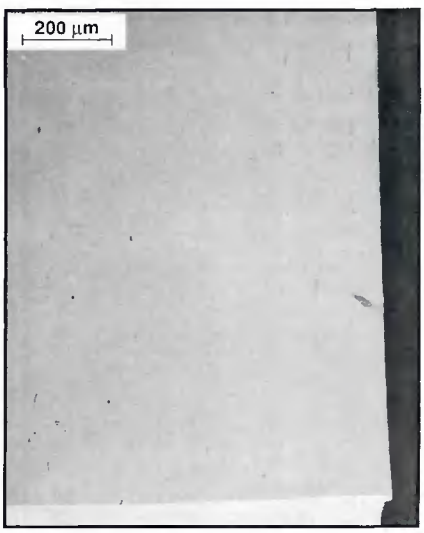

Fig. 8 — Micrograph of a deformed silver-interlayer diffusion weld (t/d = 1/42) between annealed 304 stainless steel base metals following deformation for 420 s at an applied stress of 293 MPa (42.5 ksi).

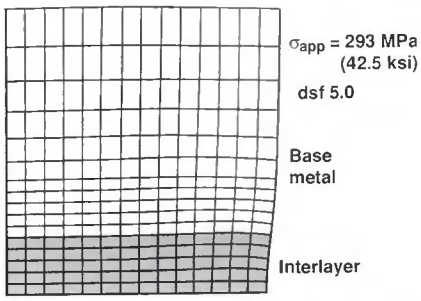

Fig. 7 — A section of the deformed mesh for a simulated silver-interlayer weld (t/d = 1/42) between annealed 304 stainless steel base metals at an applied stress of 293 MPa (42.5 ksi). All displacements have been magnified by a factor (dsf) of 5.0. The right-hand side of the mesh corresponds to the OD.

elastically deforming base metals. The vapor-deposited silver used to model the interlayer in the present study strain hardens rapidly (Fig. 2), so the effective stress within the interlayer is much larger for the weld using 304 stainless steel base metals than for the weld using maraging steel base metals, as shown in Fig. 4. Also note that the peak in $\bar{\sigma}$ near the OD is smaller for the weld between plastic base metals, which can be explained by the decreased slope of the effective stress-strain curve at large strains. The overall increase in $\bar{\sigma}$ is accompanied by a decrease in σ_r (and σ_H) relative to that for a weld using elastically deforming base metals, as shown in Fig. 6. This change in stress state significantly influences the properties of the weld. For example, Rosen and Kassner (Ref. 9) have confirmed earlier results of West, *et al.* (Ref. 2), that plastic strain in the base metal leads to a lower UTS for the weld.

Another effect of plasticity in the base metal is to increase the amount of the local plastic strain near the OD — Fig. 5. This increase is associated with the shape of the interface between the interlayer and the base metal. For an elastic base metal, the interface must remain essentially planar, limiting the amount of local plastic strain. If the base metal can deform plastically, however, the interface near the OD becomes nonplanar in the manner shown in Fig. 7, and allows for more plastic strain in the interlayer. The NIKE2D prediction of a curved interface is consistent with the shape of actual welds, as shown in Fig. 8 for a silver-interlayer weld between annealed 304 stainless steel base metals. (The low radial strain in the base metal near the interface will be discussed in the next section.) Moffatt and Wulff (Ref. 13) observed similar nonplanar interfaces near the OD in silver-interlayer welds between plain carbon-steel base metals. The consistency between the geometry predicted by NIKE2D and that observed experimentally provides confirmation that the FEM analysis is reasonably accurate.

As shown in Fig. 6, plasticity in the base metal not only decreases the overall radial (and hydrostatic) stress, but the peak in the distribution near the OD is eliminated as well. This result supports the conclusion that the peak in σ_r (and σ_H) for welds between elastic base metals is caused by the localization of interlayer plastic strain near the OD. As discussed in the previous section, for a thick interlayer weld between elastic base metals a localization of plastic strain near the OD causes an increase in the elastic strain, and therefore the principal stresses, near the center axis of the cylinder. For a thin interlayer weld, the stress increase is localized to a region just inside that at which the plastic strain is concentrated, thus producing a peak in the σ_r or σ_H distribution near the OD. For a plastic base metal, however, the large local plastic strain in the interlayer near the OD can be accommodated by plastic strain in the base metal, which leads to a curved interface such as those in Figs. 7 and 8. Therefore, the stress in not redistributed as it is for the case in which the base metals (and the interface) are essentially rigid, and the principal stress peaks are diminished or eliminated.

Time-Dependent Creep in the Base Metal

Although thin interlayer welds may have ultimate tensile strengths much larger than that of the bulk interlayer material, it has recently been demonstrated that time-dependent, or delayed, failure of the welds can occur at applied stresses much lower than the UTS of the weld (Refs. 7–10). Fig. 9 shows the data of Kassner, *et al.* (Ref. 10), for the stress dependence of the ambient-temperature creep-rupture time of 150-μm-thick (t/d = 1/42) silver-interlayer diffusion welds between two different base metals: vacuum annealed 304 stainless steel (yield stress = 221 MPa) and maraging steel (yield stress = 1518 MPa). At the applied stresses shown, the maraging steel deforms only elastically. The stainless steel, however, creeps at ambient temperature, leading to much more rapid stress-rupture. As postulated earlier (Refs. 8, 10, 18), creep of the base metal produces concomitant time-dependent shear in the interlayer. The rate of interlayer shear is controlled by the creep rate of the base metal. If this rate is faster than the creep rate of the interlayer acting under the effective stress within the interlayer (which for Ag at ambient temperature is very small, Ref. 23), then stress rupture will be accelerated by base-metal creep. Ambient-temperature creep of 304 stainless steel is reasonably well described by Equation 2 over the stress range of interest. Thus, NIKE2D simulations were performed in which the stainless steel base metal was modeled using this equation. Since the room-temperature creep rate of pure sil-

ver is much smaller than that of 304 stainless steel (Ref. 23), the interlayer was again modeled using time-independent von Mises plasticity. These simulations provide the opportunity to confirm the base-metal control theory of stress rupture proposed earlier (Ref. 8).

To assess the NIKE2D results, at least qualitatively, it was desirable to compare the shape of the deformed mesh with that of an experimentally tested weld. However, the experimentally tested welds between annealed 304 stainless steel base metals have an anomalous shape following creep deformation at room temperature. As shown in Fig. 8, the radial (and therefore axial) strain in the base metal near the interface is less than that far from the interface. This behavior is caused by machining the faces of the base metal prior to coating them with silver, which produces surface damage and increases the strength of the steel near the interface (Ref. 18).

To model the behavior of these welds, the increased strength of the base metal near the interface was accounted for, at least approximately, in the following way. First, the hardness of the base metal was measured as a function of distance from the silver interface using microhardness techniques described by Rosen (Ref. 18). Bulk samples of annealed 304 stainless steel were then strain hardened varying amounts by loading them in tension to various applied stresses. The microhardness of these samples was measured to derive an empirical relationship between hardness and tensile stress. A linear correlation, with relatively little deviation, was established (Ref. 18). Using this empirical relationship and the hardness profile from the welded sample, a curve of flow stress in the base metal vs. distance from the silver interface was constructed—Fig. 10. Since creep data at various applied stresses were already available for 304 stainless steel cold worked to 358 MPa (52 ksi), the step function shown in Fig. 10 by the solid line was used to approximate the actual

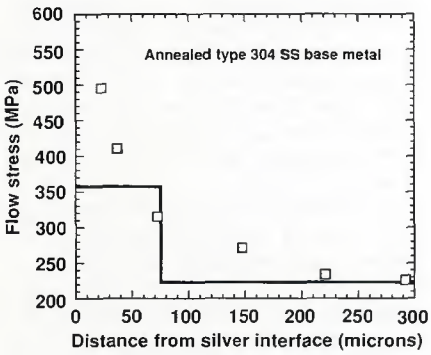

Fig. 10—The variation in strength of the 304 stainless steel base metal as a function of distance from the silver interface. The solid line shows the approximation used in the NIKE2D simulations. Data of Rosen (Ref. 18).

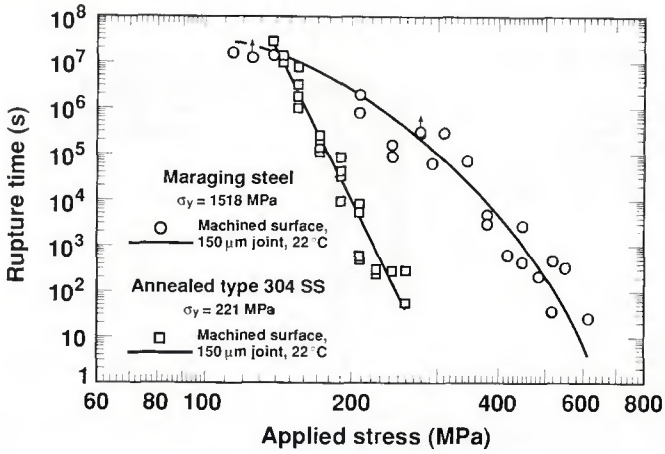

Fig. 9—Ambient-temperature creep-rupture time as a function of the applied stress for silver-interlayer diffusion welds (t/d = 1/42) between annealed 304 stainless steel and maraging steel base metals. Data of Kassner, et al. (Ref. 10).

strength-distance profile. From the creep data for cold-worked 304 stainless steel, the creep constants in Equation 2 were then evaluated. The results of this analysis gave: $A = 1.58 \times 10^{-66}$ (for stress in MPa, and time in seconds), $n = 24.76$ and $m = 0.31$. These constants were then used for the 5 rows of base-metal elements closest to the interface (75 μm or t/2), and the creep constants listed in Table 1 were used for the remaining elements in the base metal.The silver interlayer was modeled using time-independent von Mises plasticity.

To simulate a creep test, the load was applied over a period of 10 s (to avoid numerical difficulties) and then held constant at 293 MPa (42.5 ksi) for an additional 400 s. The resulting mesh shape is shown in Fig. 11, and the experimentally-tested weld is shown in Fig. 8 (t/d = 1/42 for both). Qualitatively the shapes are similar, demonstrating the success of NIKE2D and confirming the assumption that the anomalous shape is due to machining damage of the base metal interface. As expected, the strain in the base metal is smaller near the interface than far from it.

The inelastic response of the weld is shown in Fig. 12A at three positions along the center axis (r = 0) of the mesh: (a) at the center plane of the interlayer (z = 0), (b) in the base metal just above the interface and (c) in the base metal at the top of the mesh, far from the interface. The latter position represents the behavior of bulk annealed 304 stainless steel, and should correspond to that which would be obtained directly from Equation 2 for a constant stress of 293 MPa. Following 410 s of creep, there is less than 0.1% error in the effective plastic strain computed by NIKE2D compared with the

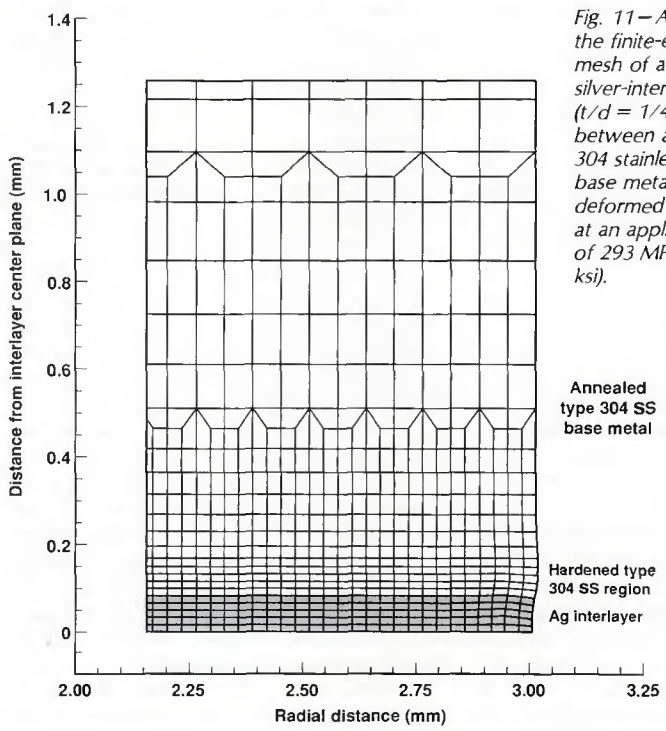

Fig. 11—A section of the finite-element mesh of a silver-interlayer weld (t/d = 1/42) between annealed 304 stainless steel base metals deformed for 410 s at an applied stress of 293 MPa (42.5 ksi).

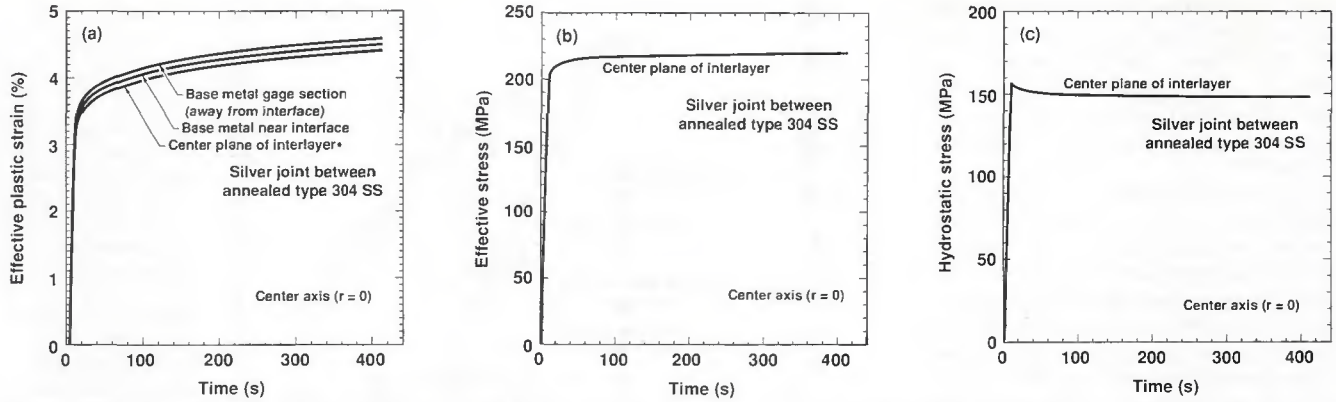

Fig. 12 — NIKE2D predictions of the time-dependence of: A — the effective plastic strain; B — the effective stress; C — the hydrostatic stress for silver-interlayer welds (t/d = 1/42) between annealed 304 stainless steel base metals.

exact solution from Equation 2. Figure 12A also shows that the creep strain in the base metal near the interface is always less than that far from the interface. The most important feature of Fig. 12A is that time-dependent creep of the base metal induces *time-dependent* plastic deformation of the interlayer, even though the interlayer alone deforms in a *time-independent* manner. Note that the creep rate of the interlayer closely follows that of the stainless steel base metal. Furthermore, following 410 s of creep, the effective plastic strain in the interlayer is much larger than if the base metal deforms only elastically, as shown by comparing Fig. 12A with the results in Fig. 5 for welds using maraging steel base metals.

Figure 12B shows the time dependence of the effective stress within the interlayer ($z = r = 0$). The effective stress is less than the applied stress (because of the triaxial stress state) but increases with time as the silver deforms and strain hardens. Again, it is creep of the base metal that reduces the triaxial constraint in the interlayer and allows the silver to deform and the effective stress to increase. In other words, creep of the base metal controls the behavior of the interlayer, and therefore the rupture time of the weld. This confirms the base-metal control theory proposed in an earlier paper by the authors (Ref.8).

For strain-hardening interlayers, another important effect of creep (or time-independent plasticity) in the base metal is that it relieves the hydrostatic stress within the interlayer. Hydrostatic tensile stresses are known to promote fracture (Refs. 21, 22), so knowledge of how σ_H changes with time and base metal properties is useful for understanding failure of the welds. For example, the relatively low σ_H in welds between plastically deforming annealed 304 stainless steel base metals may explain the relatively large fracture strains (e.g., 2-3%) compared to those for welds between elastically deforming maraging steel base metals (< 0.5%) (Ref. 9). Figure 12C shows the time dependence of σ_H at $z = r = 0$. The effect of base-metal creep in reducing σ_H is most clearly evident for times greater than 10 s; σ_H decreases for a constant applied stress. Less apparent, the large amount of creep strain during loading also effects σ_H. In total, following 410 s of creep at an applied stress of 293 MPa (42.5 ksi), σ_H is about 147 MPa. This value is 40% lower than that for a weld using maraging steel (elastic) base metals at the same applied stress, for which σ_H is 231 MPa.

Summary and Conclusions

The purpose of this investigation was to develop a quantitative understanding of the stress and strain states in thin interlayer welds loaded in tension. This study was largely motivated by recent experimental studies of time-dependent, or delayed, failure of these types of welds (Refs. 7-10). The NIKE2D FEM code was used to efficiently analyze the states of stress and strain in the interlayer for a wide variety of geometries, loading conditions and material behaviors. For the first time, the influence of base-metal plasticity, both time-independent and time-dependent, on the interlayer stress and strain states have been examined. The correlation of these results with experimental findings has been discussed. The major conclusions drawn from the FEM study are listed below.

1) For elastic base metals, the simple analytical solution for the radial stress given by Equation 1 is qualitatively correct for thick interlayers; σ_r increases roughly linearly with decreasing radial distance from the center axis of the cylindrical weld and σ_r increases as t/d decreases. Quantitatively, the radial stresses computed by NIKE2D in this case are about 50% larger than those predicted analytically. The reason for this discrepancy has been attributed to the nonuniform plastic strains in the interlayer, which are not fully accounted for in the analytical expression.

2) For thin interlayer welds between elastic base metals the radial stresses (and other principal stress components) computed by NIKE2D differ significantly from those predicted analytically or presented in an earlier FEM study on thick interlayer welds (Ref. 3). First, as t/d decreases, the principal stresses over most of the interlayer decrease, which is the opposite of that predicted analytically. Second, as t/d decreases, the stress distribution across the interlayer becomes more uniform, with a small peak occurring near the outside diameter of the cylindrical weld. Third, the sensitivity of the stress state to changes in t/d decreases rapidly as t/d decreases, consistent with experimental observations of plateaus in the strength (Refs. 9,18) and rupture life (Ref.18) vs. t/d.

3) Strain hardening in the interlayer produces stress and strain states in the interlayer that are more uniform than for an ideal plastic interlayer. Strain hardening also decreases the radial and hydrostatic stress components for a given applied stress. The transition from thick-joint to thin-joint behavior occurs at larger t/d values for strain-hardening interlayers than for ideal plastic ones.

4) Time-independent plasticity in the base metal, which partially relieves the mechanical constraint, significantly increases the amount of plastic strain in the interlayer produced by a given applied stress, particularly near the OD. For strain-hardening interlayers, such as the silver investigated in this study, the increase in interlayer plastic strain significantly alters the stress state in the interlayer. The effective stress is larger than for welds between elastic base metals, and the hydrostatic (or principal) stresses are smaller. In addition, the stress state is more uniform across the interlayer.

5) Time-dependent plasticity, or creep, of the base metal has an effect on the interlayer stress and strain state similar to that produced by time-independent plastic deformation of the base metal. In this case, creep of the base metal can induce time-dependent plastic deformation in the interlayer, even if the interlayer material alone does not creep. The creep rate of the interlayer is controlled by the creep rate of the base metal, consistent with

earlier experimental results reported by the authors in this journal.

6) By accounting for machining damage of the base metal surface, NIKE2D predictions of the geometry of a thin interlayer weld subjected to creep loading is qualitatively consistent with the shape of experimentally tested welds.

Acknowledgment

This work was performed under the auspices of the U.S. Department of Energy by Lawrence Livermore National Laboratory under contract No. W-7405-Eng-48.

References

1. Saxton, H. J., West, A. J., and Barrett, C. R. 1971. Deformation and failure of brazed joints—macroscopic considerations. *Metall. Trans:* 2:999-1007.

2. West, A. J., Saxton, H. J., Tetelman, A. S., and Barrett, C. R. 1971. Deformation and failure of brazed joints—microscopic considerations. *Metall. Trans.* 2:1009-1017.

3. Almond, E. A., Brown, D. K., Davies, G. J., and Cottenden, A. M. 1983. Theoretical and experimental interlayered butt joints tested in tension. *Int. J. Mech Sci.* 25:175-189.

4. Dini, J. W., Kelley, W. K., Cowden, W. C., and Lopez, E. M. 1984. Use of electrodeposited silver as an aid in diffusion welding. *Welding Journal* 63(1):26-s to 34-s.

5. O'Brian, M., Rice, C. R., and Olsen, D. L. 1976. High-strength diffusion welding of silver-coated base metals. *Welding Journal* 55(1):25-27.

6. Mah, G., McLeod, P. S., and Williams, D. G. 1974. Characterization of silver coatings deposited from a hollow cathode source. *J. Vac. Sci. Technol.* 11:663-665.

7. Rosen, R. S., Walmsley, D. R., and Munir, Z. A. 1986. The properties of silver-aided diffusion welds between uranium and stainless steel. *Welding Journal* 65(4):83-s to 92-s.

8. Elmer, J. W., Kassner, M. E., and Rosen, R. S. 1988. The behavior of silver-aided diffusion-welded joints under tensile and torsional loads. *Welding Journal* 67(7): 157-s to 162-s.

9. Rosen, R. S., and Kassner, M. E. 1990. Diffusion welding of silver interlayers coated onto base metals by planar-magnetron sputtering. *J. Vac. Sci. Technol. A,* 8(9):19-29.

10. Kassner, M. E., Rosen, R. S., Henshall, G. A., and King, W. E. 1989. Delayed failure of silver-aided diffusion welds between steel. *Proc. 2nd Intnl. Conf. on Brazing, High-Temperature Brazing and Diffusion Welding,* pp. 47-52.

11. Orowan, E., Nye, J. F., and Cairns, W. J. 1945. M. O. S. Armament Res. Dept. Rept., vol. 16, p. 35.

12. Bredzs, N. 1954. Investigation of factors determining the tensile strength of brazed joints. *Welding Journal* 33(2): 545-s to 563-s.

13. Moffatt, W. G., and Wulff, J. 1963. Tensile deformation and fracture of brazed joints. *Welding Journal* 42(3): 115-s to 125-s.

14. Trimmer, R. M., and Kuhn, A. T. 1982. The strength of silver-brazed stainless steel joints—a review. *Brazing & Soldering* 2:6-13.

15. Lautenschlager, E. P., Marker, B. C., Moore, B. K., and Wildes, R. 1974. Strength mechanisms of dental solder joints. *J. Dent. Res.* 53:1361-1367.

16. Hallquist, J. O. 1986. NIKE2D: An implicit, finite deformation, finite element code for analyzing the static and dynamic response of two-dimensional solids, University of California, Lawrence Livermore National Laboratory, Rept. UCRL-5267B, Rev. 1.

17. Whirley, R. G., and Henshall, G. A. 1990. Creep deformation structural analysis using an efficient numerical algorithm, submitted to *Int. J. Numer. Methods Eng.*

18. Rosen, R. S. 1990. Time-dependent failure of silver interlayer welds, Ph.D. dissertation. University of California, Davis, Calif.

19. van Rooyen, G. T., and Backofen, W. A. 1960. A study of interface friction in plastic compression. *Int. J. Mech. Sci.* 1:1-27.

20. Musin, R. A., Antisverov, V. A., Belikov, Y. A., Lyamin, Y. U., and Solokov, A. N. 1979. The effects on the strength of the joint of the thickness of the soft interlayer in diffusion welding. *Automatic Welding* 32:38-40.

21. Rice, J. R., and Tracey, D. M. 1969. On the ductile enlargement of voids in triaxial stress fields. *J. Mech. Phys. Solids* 17:201-217.

22. Hancock, J. W., and MacKenzie, A. C. 1976. On the mechanisms of ductile failure in high-strength steels subjected to multi-axial stress states. *J. Mech. Phys. Solids* 24:147-169.

23. Kassner, M. E. 1989. The rate-dependence and microstructure of high-purity silver deformed to large strains between 0.16 and 0.30 T_m. *Metall. Trans.* 20A:2001-2010.

Appendix

Symbol	Meaning
A	constant in primary creep law
D	triaxiality parameter, $3\sigma_H/2\bar{\sigma}$
d	diameter of cylindrical specimen
E	Young's modulus
m	time exponent in primary creep law
n	stress exponent in primary creep law
OD	outside diameter of cylindrical specimen
r	radial distance from the center axis
r_0	initial radius
t	interlayer thickness
z	axial distance from the interlayer mid-plane
$\bar{\epsilon}_{cr}$	effective creep strain
$\bar{\sigma}$	von Mises effective stress
σ_H	hydrostatic stress
σ_r	radial stress
σ_z	axial stress
σ_y	yield stress of bulk interlayer material
ν	Poisson's ratio
τ	time (primary creep law)

WRC Bulletin 349
December 1989

This bulletin contains two reports that evaluate the PWHT cracking susceptibility of several Cr-Mo steels and several HSLA pressure vessel and structural steels.

Postweld Heat Treatment Cracking in Chromium-Molybdenum Steels
By C. D. Lundin, J. A. Henning, R. Menon and J. A. Todd

Postweld Heat Treatment Cracking in High-Strength Low-Alloy Steels
By R. Menon, C. D. Lundin and Z. Chen

Publication of this report was sponsored by the University Research Committee of the Welding Research Council. The price of WRC Bulletin 349 is $35.00 per copy, plus $5.00 for U.S., or $10.00 for overseas, postage and handling. Orders should be sent with payment to the Welding Research Council, 345 E. 47th St., Room 1301, New York, NY 10017.